Hydrodynamic Analysis of the Human Progesterone Receptor A-Isoform Reveals that Self-Association Occurs in the Micromolar Range†

Keith D. Connaghan-Jones,‡ Aaron F. Heneghan,‡ Michael T. Miura, and David L. Bain*

Department of Pharmaceutical Sciences, University of Colorado Health Sciences Center, Denver, Colorado 80262

Received June 20, 2006; Revised Manuscript Received July 21, 2006

ABSTRACT: Human progesterone receptors exist as two functionally distinct isoforms, an 83 kDa A-receptor (PR-A) and a 99 kDa B-receptor (PR-B). The isoforms are identical except that PR-B has an additional 164 amino acids at its N-terminus. We have previously characterized the hydrodynamics and solution assembly energetics of PR-B [Heneghan, A. F., et al. (2005) *Biochemistry 44,* 9528−9537], and here we present an analysis of PR-A. At micromolar concentrations of the receptor, sedimentation velocity studies demonstrate that PR-A undergoes a concentration-dependent change in its sedimentation coefficient distribution, indicative of a self-associating system. Global analysis of data sets collected at multiple PR-A concentrations supports the presence of a hydrodynamically homogeneous 3.50 S monomer species in equilibrium with a 7.15 S dimer species. Sedimentation equilibrium analysis demonstrates that self-association can be rigorously described by a monomer−dimer assembly reaction and a dimerization free energy of -7.6 ± 0.6 kcal/mol. Both the PR-A monomer and dimer are structurally asymmetric, although the extent of asymmetry is significantly decreased for the dimer, indicative of quaternary-induced hydrodynamic compaction. Limited proteolysis studies suggest that PR-A asymmetry arises from an ensemble of partially folded conformations within the N-terminal half of the molecule. Finally, comparison to our previous work on PR-B self-association energetics demonstrates that it dimerizes, under identical solution conditions, with an affinity at least 8-fold weaker than that of PR-A. Thus, residues unique to the B-isoform destabilize receptor assembly energetics. Importantly, the physical and chemical driving forces underlying isoform-specific dimerization suggest that B-unique amino acids modulate the energetics through an allosteric mechanism.

Progesterone receptors (PRs) are members of the nuclear receptor superfamily of ligand-activated transcription factors (*1*). An understanding of PR function is complicated by the existence of two functionally distinct isoforms: an 83 kDa A-receptor (PR-A) and a 99 kDa B-receptor (PR-B) (*2*). The two proteins are identical in primary amino acid sequence except that PR-B has an additional 164 amino acids at its N-terminus (Figure 1A). Both isoforms contain a centrally located DNA binding domain (DBD) and a C-terminal hormone binding domain (HBD). Separating the two domains is a 50-amino acid "hinge" sequence of unclear function. Transcriptional activation functions are located N-terminal to the DBD (AF-1) and within the HBD (AF-2). The 164-residue B-unique sequence (BUS) contains an additional context-dependent transcriptional activation function, AF-3 (*3*, *4*).

Despite the near identity of their sequences, the two isoforms display markedly different functional properties on gene promoters and in tissue types, as follows: (1) PR-B is typically a much stronger transcriptional activator than PR-A

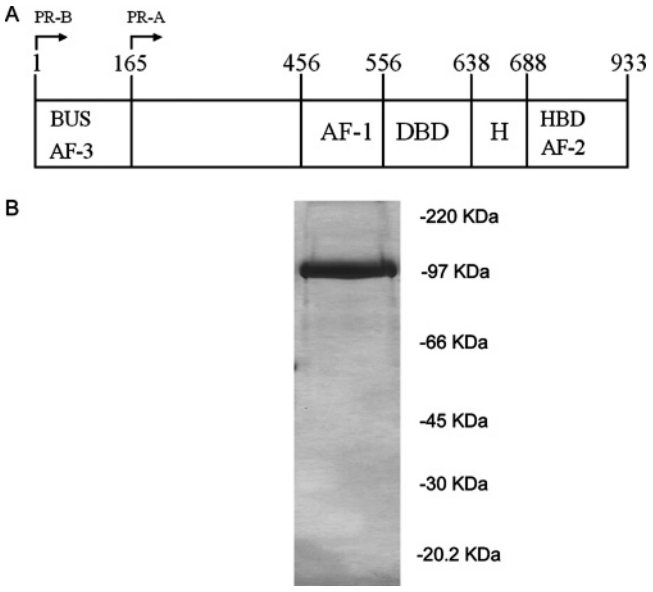

FIGURE 1: Progesterone receptor domain structure and purification of PR-A. (A) Schematic of the primary amino acid sequence for PR-A and PR-B. Functional regions are as indicated: HBD, hormone binding domain; DBD, DNA binding domain; H, hinge; AF, activation functions; BUS, B-unique sequence. PR-A is defined as amino acids 165−933. (B) Baculovirus-expressed PR-A was purified as described in Experimental Procedures. The purified protein (5 μg) was resolved by 12% SDS−PAGE and silver stained. Molecular mass standards are given at the right.

† This work was supported by NIH Grants R01-DK061933 to D.L.B. and F-32-DK070519 to A.F.H.

* To whom correspondence should be addressed: Department of Pharmaceutical Sciences, C-238, University of Colorado Health Sciences Center, 4200 E. 9th Ave., Denver, CO 80262. Phone: (303) 315-1416. Fax: (303) 315-0274. E-mail: david.bain@uchsc.edu.

‡ These authors contributed equally to this work.

10.1021/bi0612317 CCC: $33.50
Published on Web 09/07/2006

(*3*, *4*). (2) The antiprogestin RU486 acts as a partial agonist toward the B-isoform, but it is a pure antagonist toward the A-isoform (*5*). (3) PR-A "knockout" mice develop uterine dysplasia and abnormal ovaries (*6*), while PR-B gene knockouts primarily affect the mammary glands, causing premature ductal growth arrest and incomplete lobular−alveolar differentiation (*7*). (4) Microarray studies demonstrate that the two isoforms regulate different subsets of genes (*8*). (5) Finally, breast cancer patients with high PR-A:PR-B ratios relapse with greater frequency than those with low PR-A:PR-B ratios (*9*). The molecular origins of these isoform-specific functional differences are largely unknown.

Hormone-bound progesterone receptors are traditionally thought to bind as homodimers to imperfect palindromic response elements within receptor-regulated promoters (*1*). Further, biochemical studies suggest that solution homodimerization, primarily mediated by the C-terminal HBD, is a prerequisite for promoter binding (*10*, *11*). These results reflect a common property of many transcription factors, namely, the thermodynamic linkage between solution self-assembly and DNA binding energetics (*12*, *13*). This linkage can result in favorable or unfavorable contributions to DNA binding, depending upon the interaction. For example, solution dimerization may be coupled to structural transitions within the dimer that result in a more complementary stereochemical protein−DNA interface, and thus a significantly greater binding affinity, when compared to the sum of the two monomer binding affinities. However, from an experimental perspective, the nature of linked dimerization−DNA binding reactions can only be understood through explicit and independent characterization of the solution dimerization and DNA binding energetics. By contrast, macroscopic apparent binding constants (as might be determined using a gel shift assay) reflect an irreducible composite of the microscopic solution assembly and DNA binding affinities, making them problematic for understanding DNA binding mechanisms.

The importance of these types of coupled reactions can be seen in our prior analyses of PR-B solution assembly and DNA binding energetics (*14*, *15*). First, PR-B dimerization affinity ($\Delta G_{dimer} = -7.2$ kcal/mol) is in the micromolar range, in stark contrast to the nanomolar or subnanomolar affinities estimated for the closely related estrogen and glucocorticoid receptors (*16*−*18*). A functional consequence of this weak assembly reaction is that at the nanomolar concentrations at which PR-B−DNA interactions are initiated, the protein is almost entirely monomeric. Moreover, the coupling between solution dimerization and DNA binding affinity does not enhance the affinity of PR-B dimers for DNA as might be expected but in fact weakens the affinity to the point that PR-B monomers are thermodynamically favored over dimers in their ability to assemble at palindromic response elements. These results thus raise the question of whether the traditional understanding that only preformed solution dimers are the active binding species is correct and make it clear that PR-B function is considerably more complex than commonly envisioned.

As part of our effort to understand the quantitative origins of PR-B and PR-A functional differences, we have carried out a rigorous analysis of PR-A self-assembly energetics. The results of this study show that, under identical solution conditions, the two PR isoforms maintain different dimerization energetics. This difference in energetics mandates that PR-A and PR-B assembly reactions occur via different molecular mechanisms. Specifically, the HBD cannot be the sole mediator of dimerization as is often presumed, and the BUS can function to regulate PR quaternary assembly energetics. Importantly, the physical and chemical driving forces underlying isoform-specific assembly suggest that the BUS does not act as a functionally independent subunit but instead suggest that residues within the BUS allosterically modulate assembly. These studies represent the first rigorous and comparative analysis of isoform-specific self-association properties and set the stage for a detailed dissection of allosteric coupling within both PR isoforms.

EXPERIMENTAL PROCEDURES

Expression and Purification of the Intact Human Progesterone Receptor A-Isoform (PR-A). An expression vector encoding full-length PR-A (amino acids 165−933 as defined in Figure 1A) fused to an N-terminal hexahistidine tag was a generous gift of D. Edwards. PR-A was expressed in baculovirus-infected Sf9 insect cells, and whole cell extracts were prepared as previously described (*19*, *20*). Saturating concentrations of progesterone were present at all times during purification and storage, and all purification steps were carried out at 4 °C. PR-A was first partially purified using Ni^{2+}−agarose chromatography (Qiagen). Loading buffer conditions were 20 mM Bis-Tris (pH 7.0), 10% glycerol (w/v), 500 mM NaCl, 15 mM β-ME, 35 mM imidazole, and 10^{-5} M progesterone. Upon binding the receptor to the column, the resin was washed extensively with loading buffer, and the bound protein was then eluted using loading buffer containing 250 mM imidazole. The eluate from the Ni^{2+}−agarose column was loaded directly onto a Sephacryl S-200 size exclusion column equilibrated in a buffer containing 20 mM Bis-Tris (pH 7.0), 10% glycerol (w/v), 500 mM NaCl, 15 mM β-ME, and 10^{-5} M progesterone. The receptor fraction was collected, flash-frozen, and stored in liquid nitrogen. PR-A was judged to be ~95% pure by quantitation of Coomassie Blue-stained SDS−PAGE. The PR-A concentration was determined using a calculated extinction coefficient of 57 810 M^{-1} cm^{-1} (*21*). Typical yields were 1.5 mg of pure PR-A/L of culture.

Sedimentation Velocity. Sedimentation was carried out on a Beckman XL-A analytical ultracentrifuge equipped with absorbance optics. A two-channel Epon centerpiece and an An-60 Ti rotor were used for all velocity experiments. PR-A was loaded at initial concentrations of 1.5, 1.0, and 0.5 μM and sedimented at 4 °C in a buffer containing 20 mM Hepes (pH 8.0), 2.5 mM $MgCl_2$, 1 mM $CaCl_2$, 1 mM DTT, 10^{-5} M progesterone, and NaCl concentrations ranging from 100 to 1000 mM. PR-A was sedimented at a rotor speed of 50 000 rpm, with data collected at 230 nm and as quickly as the instrument would allow (typically every 4 min). The sedimentation coefficient distribution, $g(s^*)$, and weight-average sedimentation coefficient at each PR-A concentration were calculated as implemented in DCDT+ (*22*, *23*). Each distribution was corrected to 20 °C and water ($s_{20,w}$) using standard methods (*24*).

To determine the $s_{20,w}$ for each species in solution (e.g., dimer), the data collected at 300 mM NaCl were fit directly to the Lamm equation as implemented in Sedphat (*25*). Data

sets from the three initial loading concentrations were analyzed globally using a monomer−dimer assembly model. The dimerization constant and kinetic off rate were allowed to vary during the fitting process, as were the sedimentation coefficients for the monomer and dimer. The molecular masses of the monomer and dimer species were also allowed to vary with the constraint that the dimer molecular mass was twice that of the monomer. Finally, a parameter for a nonparticipating species was included in the fit to account for aggregated or incompetent material. This resolved value never exceeded 5% of the PR-A population.

The frictional coefficient (f) of each assembly species was determined using its resolved $s_{20,w}$ and the Svedberg equation:

$$s_{20,w} = M(1 - \bar{\nu}\rho)/Nf \quad (1)$$

where M is the molecular mass as calculated by the amino acid sequence and assembly stoichiometry, $\bar{\nu}$ is the partial specific volume of the protein, ρ is the water density at 20 °C, and N is Avogadro's number. The partial specific volume for PR-A was calculated by summing up the partial specific volumes of each individual amino acid (0.7302 mL/g) (*26*). To calculate a frictional ratio for each species, the frictional coefficient of a compact sphere of the same molecular mass (f_0) was calculated assuming a degree of hydration of 0.3 g of water/g of protein (*27*, *28*).

Sedimentation Equilibrium. Sedimentation equilibrium was carried out at 300 mM NaCl and otherwise identical buffer and temperature conditions as described for the sedimentation velocity experiments. Samples were allowed to reach sedimentation equilibrium in a Beckman XL-A ultracentrifuge using six-channel Epon centerpieces. Samples were equilibrated at 15 000, 18 000, and 21 000 rpm and judged to be at equilibrium by successive subtraction of scans. Three PR-A concentrations were analyzed at a ratio of 4:2:1, with the highest loading concentration being 1.0 μM. The nine data sets (three concentrations collected at three rotor speeds) were analyzed by nonlinear least-squares (NLLS) parameter estimation as implemented in NONLIN (*29*). Each data set was first analyzed individually to resolve σ, the reduced molecular mass, using the equation

$$Y_r = \delta + \alpha \exp\left[\sigma\left(\frac{r^2 - r_0^2}{2}\right)\right] \quad (2)$$

where Y_r is the absorbance at radius r, δ is the baseline offset, and α is the absorbance at the reference radius, r_0. σ, the reduced molecular mass, is defined as

$$\sigma = M(1 - \bar{\nu}\rho)\omega^2/RT \quad (3)$$

where M is the weight-average molecular mass of a single, ideal species, $\bar{\nu}$ is the partial specific volume, ρ is the solvent density [as calculated on the basis of the salt composition and temperature (*30*)], ω is the angular velocity, R is the gas constant, and T is the temperature in kelvin.

For data sets in which the weight-average molecular mass, M, increased with an increase in protein concentration, the data were analyzed globally to resolve self-association equilibrium constants:

$$Y_r = \delta + \alpha \exp\left[\sigma\left(\frac{r^2 - r_0^2}{2}\right)\right] + \sum \alpha^N K_N \exp\left[N\sigma\left(\frac{r^2 - r_0^2}{2}\right)\right] \quad (4)$$

where Y_r is absorbance at radius r, δ is the baseline offset, and α is the monomer absorbance at the reference radius, r_0, σ is the reduced molecular mass (eq 3), N is the stoichiometry of the reaction, and K_N is the association constant of the $N \cdot M \leftrightarrow M_N$ reaction. The σ for global analysis was fixed at the value of the PR-A monomer as calculated by its amino acid composition. Resolved values of K_N were converted from absorbance to molar association constants on the basis of the calculated ϵ_{230}. Free energies for the assembly reactions were calculated using the relation $\Delta G_N = -RT \ln K_N$.

Limited Proteolysis. Sequencing-grade EndoGluC, EndoLysC, and chymotrypsin were obtained from Roche Applied Science. PR-A (1 μM) was digested under buffer and temperature conditions identical to those described for the 300 mM NaCl sedimentation velocity and sedimentation equilibrium studies. Enzyme was added at a PR-A:enzyme mass ratio of 50:1 for EndoGluC and EndoLysC; enzyme was added at a ratio of 1000:1 for chymotrypsin. Each reaction was allowed to proceed for 90 min with aliquots removed as a function of time. Reactions were terminated by addition of SDS−PAGE loading dye and boiling for 5 min; 5 μg of PR-A was electrophoresed via 10% SDS−PAGE and either silver-stained or transferred to a PVDF membrane for Edman degradation microsequencing analysis (Molecular Resource Center, National Jewish Center for Immunology, Denver, CO). Microsequencing was carried out for 7−10 cycles to identify enzymatic cleavage sites. Antibodies used for analysis were α266, a polyclonal antibody raised against a peptide corresponding to DNA binding domain residues V611−C627 [generously donated by D. Toft (*31*)]; C-19, a polyclonal antibody specific for the C-terminal portion of the PR hormone binding domain (Santa Cruz Biotechnology, Inc.); and Anti-His, an antibody specific for the hexahistidine sequence located at the N-terminus of PR-A (GE Healthcare).

RESULTS

Milligram quantities of PR-A (Figure 1A) were purified from baculovirus-infected Sf9 cells using the two-column chromatographic scheme described in Experimental Procedures (Figure 1B). SDS−PAGE analysis showed that PR-A was at least 95% pure by densitometric scanning of Coomassie Blue-stained gels (not shown). In addition, the purified protein was immunoreactive to antibodies specific for the N-terminal hexahistidine sequence and the C-terminal HBD, thus demonstrating that the protein was not significantly proteolyzed or degraded during purification and storage. Finally, we note that our previous work on PR-B and PR deletion constructs indicates that the hexahistidine tag has no detectable influence on the gross structural properties of the protein (*32*, *33*) and that the tagged receptor maintains high functional activity (*14*, *15*).

Sedimentation Velocity Demonstrates that PR-A Undergoes Dynamic Self-Assembly. Sedimentation velocity was used to examine the hydrodynamic properties of PR-A as a

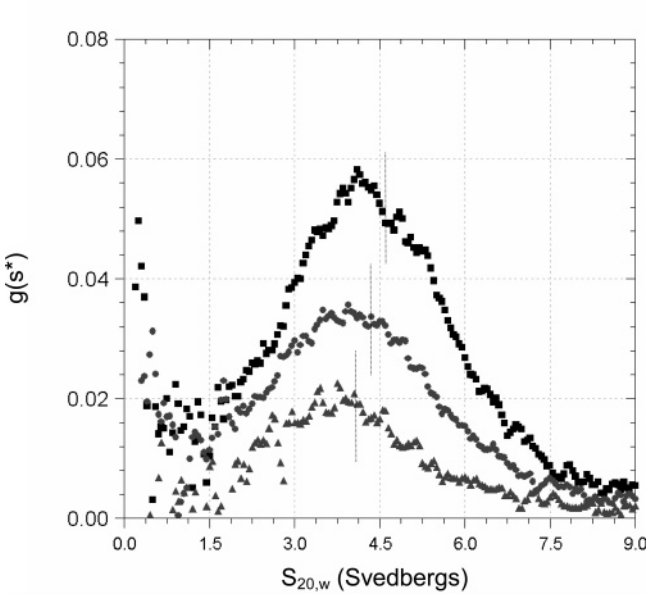

FIGURE 2: Concentration dependence of $g(s^*)$ distributions for PR-A. Initial loading concentrations were 1.5 (■), 1.0 (●), and 0.5 μM (▲). $g(s^*)$ distributions were determined by analysis of successive scans taken at each loading concentration. Vertical dashed lines indicate the weight-average sedimentation coefficient determined by analysis of each $g(s^*)$ distribution. The buffer consisted of 20 mM Hepes (pH 8.0), 300 mM NaCl, 2.5 mM $MgCl_2$, 1 mM $CaCl_2$, 1 mM DTT, and 10^{-5} M progesterone at 4 °C.

function of protein concentration. These studies were carried out at monovalent salt concentrations ranging from 100 to 1000 mM NaCl and at three PR-A concentrations (1.5, 1.0, and 0.5 μM). In the course of analysis, it was found that NaCl concentrations below 300 mM decreased the solubility of PR-A. For the PR-A samples at 1.5 μM, the aggregating fraction was approximately 5% at 200 mM NaCl and 15% at 100 mM NaCl, as judged by monitoring the initial decrease in sedimentation velocity plateau absorbance values. Since the pI of the protein is 8.02 and the solution pH is 8.0, we speculate that protein loss under low-salt conditions is simply due to a decreased solubility limit for the receptor, rather than an ionic linkage to soluble self-assembly. Consistent with this result, PR-A samples at 1.0 and 0.5 μM showed no evidence of insoluble material regardless of NaCl concentration. As a consequence, global analysis of data sets from all three PR-A concentrations could be carried out only at NaCl concentrations of ≥300 mM. Representative results obtained at 300 mM NaCl are presented below.

Figure 2 shows the sedimentation coefficient distribution, $g(s^*)$, calculated from the data for three PR-A concentrations (1.5, 1.0, and 0.5 μM). The temperature- and buffer-corrected sedimentation coefficient distribution shifts from a weight-average $s_{20,w}$ of 4.6 ± 0.2 at the highest protein concentration to an $s_{20,w}$ of 4.1 ± 0.1 at the lowest protein concentration. A concentration-dependent shift in the sedimentation coefficient is a hallmark of a self-associating system. This possibility was tested rigorously using sedimentation equilibrium as described below.

Sedimentation Equilibrium Confirms a Reversible Monomer−Dimer Assembly Reaction. Panels A−C of Figure 3 show the results of a series of nine sedimentation equilibrium experiments (three PR-A concentrations equilibrated at three rotor speeds), carried out under solution conditions identical to those of the 300 mM NaCl sedimentation velocity experiments. The three concentrations consist of PR-A loading concentrations in a ratio of 4:2:1 with the highest loading concentration being 1 μM. Each concentration was allowed to reach equilibrium at three rotor speeds (15 000, 18 000, and 21 000 rpm). Individual analyses of the data sets using a single-species model (eqs 2 and 3) revealed that the weight-average molecular mass of the receptor population increased as a function of increasing protein concentration. This observation is indicative of dynamic protein self-assembly. Consistent with this, attempts to globally fit the nine data sets to a nonassociating, monomer model resulted in a poor quality of the fit (square root of the variance of 0.021 absorbance unit). Moreover, the fitted σ parameter was determined to be roughly 1.5 times the calculated value of the monomer. We then analyzed the data globally using a monomer−dimer equilibrium model, which resulted in a significantly improved fit (square root of the variance of 0.010 absorbance unit), and randomly distributed residuals (Figure 3). Moreover, if allowed to vary, the σ parameter returned a value of 2.30, in close agreement with the calculated value of 2.29. Using this model, the dimerization free energy for PR-A was determined to be −7.6 ± 0.6 kcal/mol, which corresponds to a dissociation constant of 1.08 μM at 4 °C. Attempts to fit the data to more complex interaction models (i.e., monomer−dimer−trimer) resulted in either no improvement in fit, a poorer quality of fit, or failure to converge, indicating the monomer−dimer assembly scheme is most appropriate to describe the data.

Direct Fitting of the Sedimentation Velocity Data: PR-A Exists as Two Asymmetric Structures. Both the sedimentation equilibrium and velocity results support a monomer−dimer assembly reaction occurring in the low micromolar range. As a consequence, the peak $s_{20,w}$ values seen in Figure 2 and weight-average $s_{20,w}$ values discussed in the text do not correspond to any discrete species in solution. Rather, the values reflect the composite averages of the individual monomer and dimer contributions. To address the molecular properties of the PR-A monomer and dimer species, the sedimentation velocity data collected at 300 mM NaCl were fit directly to the Lamm equation as implemented in Sedphat (*25*). On the basis of the sedimentation equilibrium results, the three velocity data sets were fit globally to an interacting monomer−dimer assembly reaction (Figure 4A−C). The data were described well by this model, as judged by a local rmsd of 0.0037 absorbance unit and randomly distributed residuals (Figure 4D−F). Global analyses using either a noninteracting model or various higher-order models (e.g., monomer−trimer) resulted in a poorer quality fit or unrealistic hydrodynamic parameters. Thus, using the monomer−dimer model, the $s_{20,w}$ of the monomer was determined to be 3.50 S and that of the dimer was 7.15 S. The resolved monomeric molecular mass was 81 981 Da, in good agreement with the calculated value of 82 295 Da. Similarly, the equilibrium dissociation constant was determined to be 2.3 μM, in reasonable agreement with the 1.08 μM constant resolved by sedimentation equilibrium. Finally, the kinetic off rate for dimer dissociation was determined to be 0.0042 s^{-1}, which corresponds to a $t_{1/2}$ of 29 min. The concordance between the velocity results and equilibrium results suggests that both the PR-A monomer and dimer are structurally homogeneous; making this assumption allows us to mean-

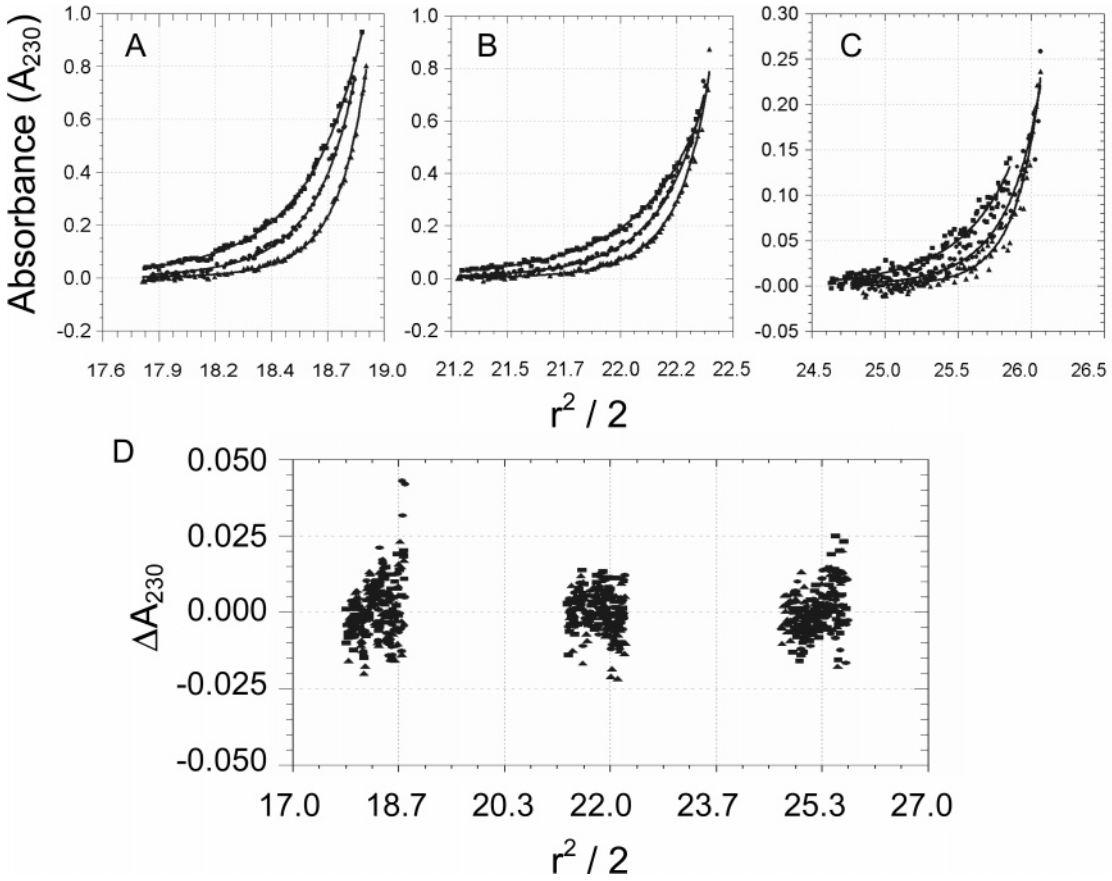

FIGURE 3: Sedimentation equilibrium analysis of PR-A plotted as the absorbance vs radius^2/2. Panels A−C represent each initial loading concentration: 1.0 (A), 0.5 (B), and 0.25 μM (C). Symbols represent PR-A absorbance at 15 000 (■), 18 000 (●), and 21 000 rpm (▲). Solid lines represent the best fit model (monomer−dimer) from simultaneous analysis of all nine data sets. The square root of the variance was 0.010 absorbance unit. Panel D shows residuals from the monomer−dimer equilibrium model plotted as a change in absorbance versus radius^2/2. The buffer consisted of 20 mM Hepes (pH 8.0), 300 mM NaCl, 2.5 mM $MgCl_2$, 1 mM $CaCl_2$, 1 mM DTT, and 10^{-5} M progesterone at 4 °C.

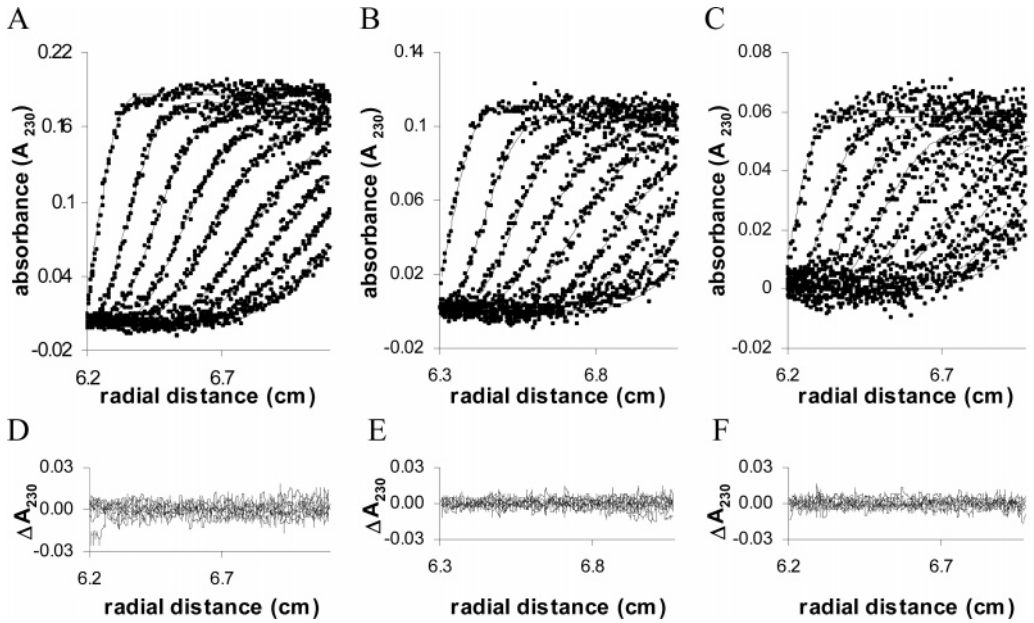

FIGURE 4: Direct fitting of PR-A sedimentation velocity data to the Lamm equation. Initial protein loading concentrations were 1.5 (A), 1.0 (B), and 0.5 μM (C). Squares represent scans of PR-A at 50 000 rpm plotted as a function of time and radial position. Solid lines represent a global analysis to all three data sets using a monomer−dimer equilibrium model. The rmsd for the fit was 0.0037 absorbance unit. Panels D−F represent the residuals of the fit for data sets A−C, respectively. For clarity, only every other scan from the global analysis is shown.

ingfully interpret the hydrodynamic parameters in terms of molecular properties as described below.

The hydrodynamic properties of the monomer and dimer were calculated using the Svedberg equation (eq 1) and the

Table 1: Hydrodynamic and Thermodynamic Properties of PR-A Determined by Analytical Ultracentrifugation[a]

	PR-A monomer	PR-A dimer
$s_{20,w}$	3.5	7.15
f (g/s)	1.06×10^{-7}	1.04×10^{-7}
f/f_0	1.70	1.32
Stokes radius (Å)	56	55
axial ratio	15:1	6:1
M_w (Da)[b]	81981	163962
equilibrium dissociation constant (μM)[b]	2.3	−
equilibrium dissociation constant (μM)[c]	1.1	−

[a] The buffer consisted of 20 mM Hepes (pH 8.0), 300 mM NaCl, 2.5 mM $MgCl_2$, 1 mM $CaCl_2$, 1 mM DTT, and 10^{-5} M progesterone at 4 °C. [b] Determined from direct fitting of analytical ultracentrifugation data and a monomer−dimer equilibrium model using Sedphat. [c] Determined by sedimentation equilibrium.

molecular mass of each species. The frictional coefficient of the monomer was calculated to be 1.06×10^{-7} g/s, with a Stokes radius of 56 Å. Comparison of the frictional coefficient to that of a rigid sphere of the same molecular mass resolved a frictional ratio (f/f_0) of 1.70, indicative of significant structural asymmetry. If modeled as a hydrated prolate ellipsoid, the monomer has a major:minor axial ratio of approximately 15:1. By comparison, the frictional coefficient of the PR-A dimer was 1.04×10^{-7} g/s with a Stokes radius of 55 Å. These values, similar to that of the monomer but describing a molecule of twice the molecular mass, cause the frictional ratio of the dimer to be significantly decreased, having a value of only 1.32. This more moderate asymmetry predicts a prolate ellipsoid axial ratio of approximately 6:1 and indicates that the PR-A dimer maintains a significantly more compact hydrodynamic structure than the monomer. A complete summary of the hydrodynamic and thermodynamic parameters for PR-A is presented in Table 1.

PR-A Self-Association Appears To Be Insensitive to NaCl Concentration. To assess any electrostatic contribution to PR-A dimerization, we carried out sedimentation velocity studies over a range of NaCl concentrations. Shown in Figure 5 is the weight-average $s_{20,w}$ of PR-A as a function of NaCl concentration, at initial loading concentrations of 1.0 μM (as noted earlier, PR-A solubility is unaffected at this protein concentration). It is evident that concentrations ranging from 100 to 1000 mM have no perceivable affect on the sedimentation coefficient and thus suggest that NaCl does not influence PR-A self-association properties. However, to rigorously confirm this hypothesis, the energetics of PR-A assembly as a function of NaCl concentration will need to be determined via sedimentation equilibrium.

Limited Proteolysis Demonstrates that Hydrodynamic Asymmetry Is Due to a Nonglobular Conformational Ensemble Localized to the N-Terminal Region. To probe the structural origins of PR-A dimerization and hydrodynamic asymmetry, we carried out limited proteolysis studies under conditions identical to those used for the 300 mM NaCl sedimentation velocity and equilibrium studies. Figure 6A shows the results of three proteolysis reactions using Endo-GluC, chymotrypsin, and EndoLysC. It is evident that regardless of enzyme, PR-A is degraded into a number of stable fragments with molecular masses ranging from approximately 15 to 70 kDa. Microsequencing of the fragments via Edman degradation (fragments 1−3 and 5−13) or immunoblotting (fragments 4 and 14) reveals that the

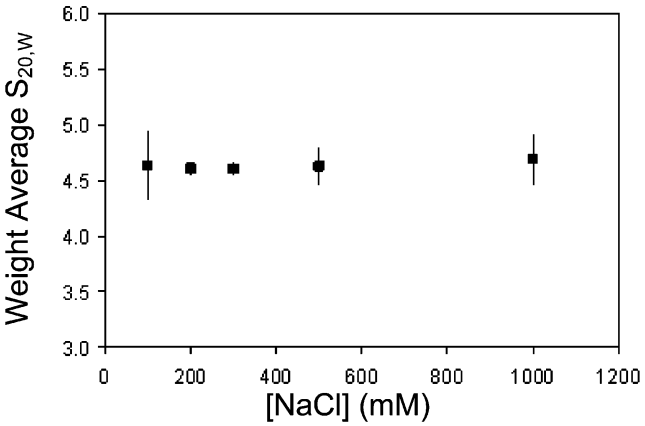

FIGURE 5: Weight-average $s_{20,w}$ for PR-A as a function of NaCl concentration. Solid squares represent the weight-average $s_{20,w}$ as calculated from the $g(s^*)$ distribution as a function of NaCl concentration. Error bars represent one standard deviation. The PR-A concentration at all NaCl concentrations was 1 μM.

majority of sites accessible to enzymatic attack are located at residues between the N-terminus and the DBD, and often close to the AF-1 functional boundary (fragments 1−3, 5−7, and 10−12; see Figure 6B). The widespread proteolytic attack in the N-terminal region is suggestive of a partially folded, nonglobular conformational ensemble, consistent with the hydrodynamic asymmetry seen by sedimentation velocity analysis. Further, since the microsequencing results reveal that only C-terminal fragments maintain stability, the immediate disappearance of the corresponding N-terminal fragments demonstrates that these sequences must immediately lose any residual structure upon cleavage from the holoprotein. This phenomenon was observed previously using PR constructs lacking only their HBD (*32*, *33*) and indicated that N-terminal structural properties were somehow modulated by interactions with the DBD. Finally, the cleavage sites at the C-terminal end of the molecule map only to the hinge sequence (fragments 8, 9, and 13) and thus define the boundary of the highly folded and globular HBD and DBD (*1*).

DISCUSSION

Energetics of PR Self-Association. As noted in the introductory section, a property of many transcription factors is that their solution assembly is often thermodynamically linked to DNA binding. As such, any mechanistically meaningful analysis of protein−DNA binding interactions must explicitly account for the self-association energetics. In the absence of this information, only macroscopic apparent binding affinities can be resolved, and these have little utility in attempting to understand DNA binding mechanisms. Using sedimentation velocity, we demonstrate that PR-A self-associates in the micromolar range, undergoing a concentration-dependent change in its weight-average $s_{20,w}$ (Figure 2). Rigorous sedimentation equilibrium studies (Figure 3) resolved a dimerization free energy change of -7.6 ± 0.6 kcal/mol, equivalent to a dimerization dissociation constant of 1.08 μM. Direct fitting of the sedimentation velocity data (Figure 4) is in clear agreement with these results. This weak dimerization constant, determined in the presence of saturating amounts of progesterone, is also consistent with the relatively small (700 Å^2) dimerization interface seen for the progesterone-bound PR-HBD structure (*34*).

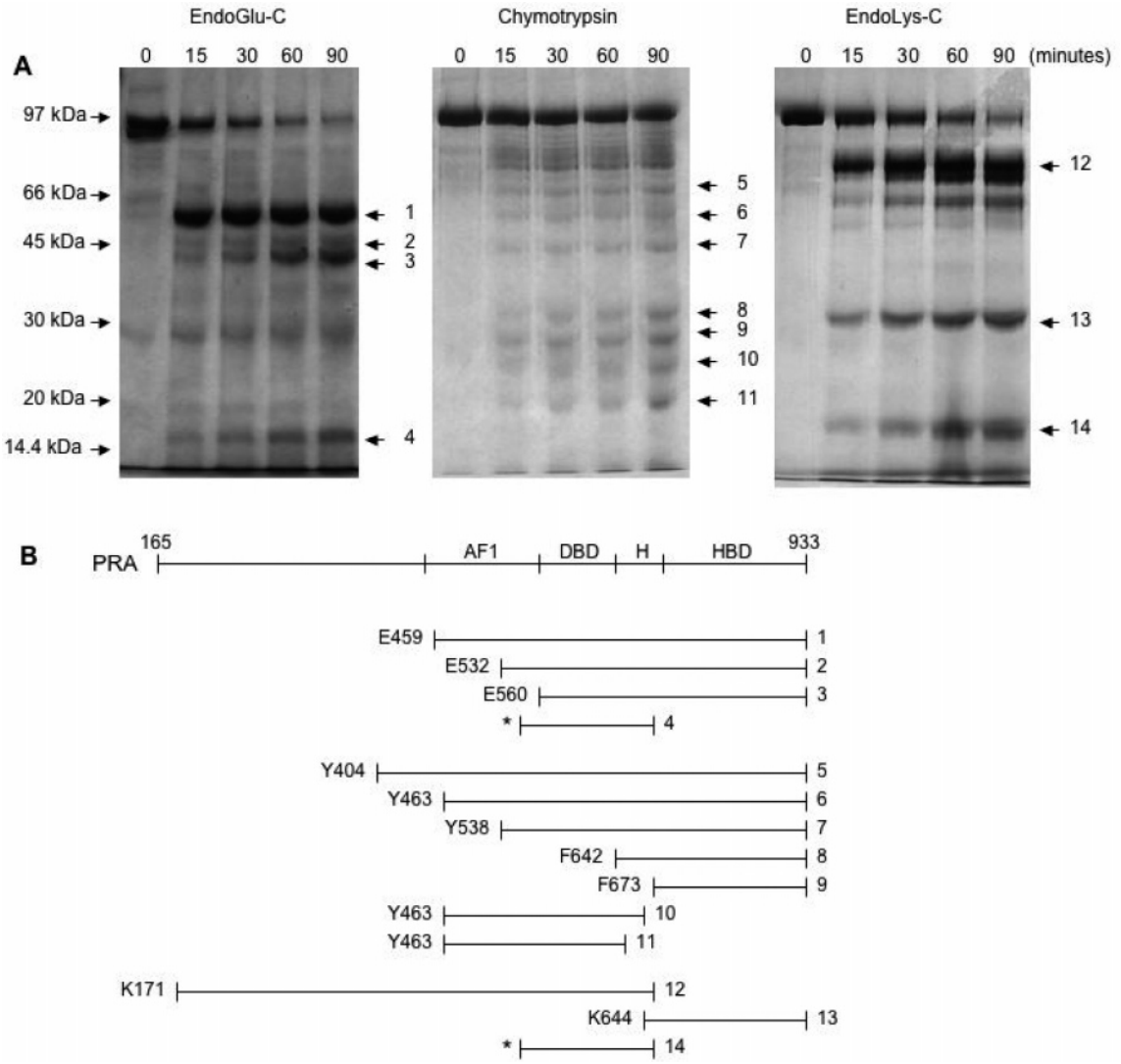

FIGURE 6: Time course for EndoGluC, chymotrypsin, and EndoLysC digestion of PR-A and mapped proteolytic fragments. (A) Purified PR-A (1 μM) was digested with EndoGluC, chymotrypsin, or EndoLysC for 0−90 min at pH 8.0 in 300 mM NaCl, 2.5 mM $MgCl_2$, 1 mM $CaCl_2$, 1 mM DTT, and 10^{-5} M progesterone at 4 °C. Resultant peptides were resolved and visualized using silver-stained SDS−PAGE. Molecular mass markers are given at the left. Major digestion products analyzed by microsequencing or immunoblotting are denoted with arrows. (B) Schematic of the intact PR-A amino acid sequence and PR-A digestion products. N-Termini of proteolytic fragments were determined by microsequencing as indicated or by immunoblot analysis (*); C-termini were estimated by immunoblot analysis and apparent molecular mass.

Driving Forces Underlying PR-A Self-Association. The physical and chemical forces responsible for PR-A dimerization energetics remain somewhat unclear. Sedimentation velocity analyses carried out over a 10-fold range of NaCl concentration showed no evidence of an ionic contribution to self-association (Figure 5) and may suggest that hydrophobic interactions dominate the dimerization reaction. Indeed, inspection of the PR-HBD crystal structure shows that the dimer interface is made up of a number of van der Waals contacts, predictive of hydrophobic interactions (*34*). Consistent with this, velocity studies of PR-A carried out at higher temperatures show an increase in the weight-average $s_{20,w}$, suggestive of a positive enthalpy contribution (data not shown). Whether protons play a role in regulating PR-A self-association remains unclear. Sedimentation studies carried out at pH 7.0 generated results identical to those at pH 8.0, but studies at pH 6.0 caused significant protein aggregation (data not shown). Studies at more alkaline pH values are underway. Finally, it is worth noting that the isolated PR-HBD is monomeric in solution (*34*), as are highly purified PR constructs lacking the HBD (*32*, *33*). The fact that only the holoprotein self-associates suggests that dimerization is a global property of the receptor even if the HBD provides the sole dimerization surface. Thus, the forces that drive assembly, hydrophobic or otherwise, may be coupled to structural changes or interactions far beyond the actual dimerization interface.

Functional Consequences of a Micromolar Dimerization Constant. The micromolar dimerization affinity reported here has important implications for mechanisms of PR-A−DNA binding interactions. As noted in the introductory section, the traditional understanding of PR function is that hormonal ligand binding and solution dimerization are prerequisites for response element binding, and thus transcriptional activation (*1*). However, since the apparent DNA binding affinity of PR is in the nanomolar range (*15*) and intracellular receptor concentrations are thought to be in the nanomolar range (*35*), essentially all liganded PR-A in solution (99.9%)

would be monomeric, given the micromolar dimerization constant determined here. Keeping in mind that a nanomolar estimate of intracellular PR concentration can be taken only as an approximate guide due to macromolecular compartmentalization and crowding effects, it is nonetheless tempting to speculate that PR-A dimerization does not precede binding to DNA response elements. That is, in vivo, the functionally active species is the monomer. This hypothesis is consistent with recent computational analyses indicating that naturally occurring PR-regulated promoters do not contain an abundance of clearly recognizable palindromic response elements but instead are comprised of clustered half-sites that may or may not have an adjacent, and only moderately conserved, half-site (B. M. Jacobsen and K. B. Horwitz, personal communication). Rigorous kinetic analyses will be necessary to assess the time-dependent mechanism of PR-A−response element interactions.

Hydrodynamic and Structural Properties of PR-A. Direct fitting of the sedimentation velocity data (Figure 4) resolved a 3.50 S monomer species and a 7.15 S dimer species. As seen in Table 1, both of these species are highly asymmetric. This asymmetry (i.e., deviation from a tightly packed, rigid sphere) might arise from a literal nonspherical structure (e.g., rodlike), a natively unfolded or disordered conformation, or a significantly increased hydration shell. Each of these possibilities would lead to an increased apparent volume and thus increased frictional resistance during sedimentation. In the case of PR-A, the limited proteolysis studies (Figure 6) best support the second hypothesis, suggesting that residues N-terminal to AF-1 exist as an ensemble of partially or weakly folded conformations. This interpretation is consistent with previous studies on PR deletion constructs (*32*, *33*) and studies of other nuclear receptor N-terminal sequences (*36*−*38*).

PR-A dimerization results in a structure significantly less asymmetrical (frictional ratio of 1.32) than the PR-A monomer (frictional ratio of 1.70), indicative of a more hydrodynamically compact conformation. Two possibilities might explain this result. (1) Either dimerization is coupled to large-scale folding reactions within the N-terminal sequences, resulting in structural compaction and thus a decreased protein volume, or (2) the quaternary structure of the dimer forms in such a way to minimize frictional resistance relative to the monomer. Given that the results of PR-A-limited proteolysis are qualitatively similar to that seen for PR-B and the HBD-truncated PR isoforms (*14*, *32*, *33*), the second explanation is more likely. With only the macroscopic hydrodynamic parameters listed in Table 1, it is impossible to state the exact nature of the quaternary structure. However, it is reasonable to suggest that dimer formation probably does not occur via an extremely asymmetric "end-to-end" assembly reaction, for example. Clearly, a high-resolution structure of the intact receptor will be necessary to more accurately link the hydrodynamics with any particular quaternary-induced conformation.

As discussed above, the results of the PR-A-limited proteolysis studies (Figure 6A) are qualitatively consistent with previous work on PR-A lacking only its C-terminal HBD [defined as NTA (*32*)]. However, close inspection of the proteolysis results for PR-A and NTA suggests that the HBD can affect N-terminal structure. Shown in Figure 7 is a schematic summary of the microsequencing results seen

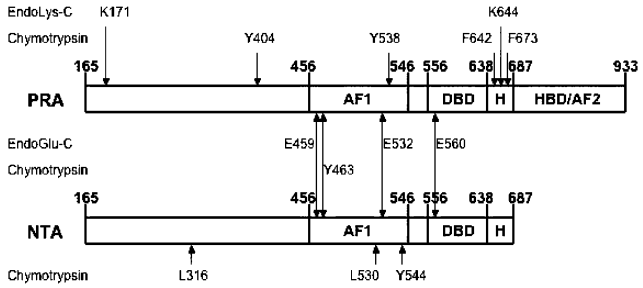

FIGURE 7: Schematic summary of proteolytic cleavage sites for PR-A and NT-A. PR-A cleavage sites were determined by microsequencing analysis for PR-A (top) and NT-A (bottom). Sites mapped by microsequencing are denoted with arrows. Sites common to both proteins are denoted with double-sided arrows interior to the schematics. Sites unique to each protein are denoted with arrows exterior to the schematics.

for PR-A (Figure 6B) and the analogous results found for NTA (*32*). It is evident that the two proteins share a number of proteolytic sites, including all the mapped EndoGluC sites (E459, E532, and E560). By contrast, chymotrypsin cleaves at a number of different residues in PR-A, including Y404 and Y538 instead of residues L316, L530, and Y544 in NTA. These results are not due to differences in buffer conditions or enzymatic concentrations since control experiments with NTA (generously donated by K. Horwitz) under identical conditions generated the results published previously (data not shown). Rather, the patterns suggest that the HBD directly, or indirectly via the influence of the progesterone ligand, subtly modulates AF-1 and N-terminal structure. Alternatively, the proteolytic differences may be due to quaternary-induced changes in structure, since at the concentration of 1 μM used in the proteolysis studies, PR-A exists in an approximately 1:1 monomer:dimer ratio (K_{dim} = 1.08 μM; see Table 1), while NTA is exclusively monomeric (*32*). However, a mixed population of monomers and dimers would predict enzymatic cleavage at the previously identified residues in NTA, something not observed in the data. Regardless of mechanism, the proteolytic differences may lend insight into studies demonstrating that N-terminal AF-1 and C-terminal AF-2 of PR can transcriptionally synergize as part of promoter activation (*39*), possibly due to mutual structural interactions or transitions.

Comparison of PR-A and PR-B Dimerization Energetics: The Role of the BUS. At 300 mM NaCl, PR-A has a dimerization dissociation constant of 1.08 μM. By contrast, our previous work on PR-B demonstrated that under the identical solution conditions, the B-isoform was entirely monomeric (*14*). Data analysis indicated that the dimerization dissociation constant for PR-B was minimally 8.8 μM, or at least 8-fold weaker than that of PR-A. This difference in dimerization energetics is not due to differences in the purification or preparation of the two isoforms, since each of the PR-A and PR-B assembly states is hydrodynamically homogeneous and functionally active under these conditions. Rather, the difference in energetics reflects inherently different molecular contributions to the respective assembly reactions. Since the two isoforms are identical in primary sequence except for the first 164 amino acids of PR-B (BUS; see Figure 1A), these residues are somehow responsible for the difference in PR isoform assembly energetics.

Several mechanisms come to mind in explaining the weaker dimerization energetics of PR-B compared to PR-A. The simplest interpretation is that the highly negatively charged B-unique sequence (pI = 4.02) destabilizes the PR-B dimer due to charge repulsion between the acidic side chains of each protomer. This explanation then predicts that increasing salt concentration should favor PR-B dimer assembly due to Debye−Huckel screening of like charges. However, our work on PR-B demonstrates that the opposite is true; an increased NaCl concentration results in dimer dissociation rather than association, leading to the release of at least 1.7 net thermodynamic ions (*14*). Given this result, a second hypothesis might be that charge attraction between the acidic side chains and the few basic side chains of each BUS subunit modulates PR-B dimerization energetics. However, this hypothesis predicts that at low salt concentrations, charged residues within the BUS should promote PR-B dimerization affinity beyond that found for PR-A. Once again, this is contradicted by the data since the dimerization affinities of PR isoforms likely converge under these conditions: The free energy change for PR-B dimerization at 50 mM NaCl is −7.2 kcal/mol (*14*), and extrapolation of the PR-A hydrodynamic results (Figure 5) to this salt concentration suggests that PR-A dimerization energetics remain constant at −7.6 kcal/mol.

Since the two isoforms dimerize by different mechanisms, an intriguing question relates to how this difference might influence PR-A−PR-B heterodimer formation (*40*). Unfortunately, experimental analyses of the energetics and hydrodynamics of heteroprotein interactions are quite difficult, since this would minimally require independent labeling of the isoforms for deconvolution of the sedimentation absorbance signals. More problematic is the fact that each absorbance signal would likely reflect heterodimer, homodimer, and monomer populations, making mathematical analysis problematic.

The arguments given above suggest that PR-B self-association properties cannot be reduced to a sum of independent (i.e., additive) BUS and PR-A properties. Rather, the data suggest that PR-B and PR-A self-association energetics differ due to a nonlinear, likely allosterically coupled, process mediated by the BUS. What this might mean from a functional perspective is only beginning to be elucidated. However, allosteric regulation by residues unique to the BUS is in accordance with evidence that BUS can modulate isoform-specific DNA binding energetics at PR-regulated promoters. Thus, PR-B interactions at a multisite promoter are characterized by surprisingly large intrinsic binding energetics and cooperative interactions, but also extremely weak DNA-induced dimerization energetics [−0.9 kcal/mol (*15*)]. By contrast, analysis of PR-A−DNA binding interactions reveals weaker intrinsic binding energetics and more attenuated cooperative interactions compared to those of PR-B, but similar DNA-induced dimerization energetics (K. D. Connaghan-Jones, A. F. Heneghan, M. T. Miura, and D. L. Bain, manuscript in preparation). This difference in energetics translates into the decreased occupancy of PR-A at the promoter compared to that of PR-B and may thus offer insight into the decreased transcriptional activation properties of the A-isoform (*4*). However, the similarly weak DNA-induced dimerization energetics seen for both isoforms, significantly lower than the solution dimerization free energy presented here, indicates that the BUS does not play a role in modulating this effect. How these events might occur at the structural level remains unclear, although earlier work suggesting that the BUS modulates the conformational ensemble of PR N-terminal sequences by stabilizing a more functionally active set of conformations (*33*) may offer a framework for future analysis.

In summary, these studies suggest that progesterone receptors, though made up of modular structural and functional subunits, function as complex allosteric transcription factors. A major challenge will be to more precisely connect the observed energetics with the structural transitions that are functionally significant.

ACKNOWLEDGMENT

We thank Dr. Dean Edwards for constructs and Drs. Kathryn Horwitz and David Toft for reagents. We also thank Drs. Carlos Catalano, N. Karl Maluf, and Peter Schuck for helpful discussions.

REFERENCES

1. Tsai, M. J., and O'Malley, B. W. (1994) Molecular mechanisms of action of steroid/thyroid receptor superfamily members, *Annu. Rev. Biochem. 63*, 451−86.
2. Kastner, P., Krust, A., Turcotte, B., Stropp, U., Tora, L., Gronemeyer, H., and Chambon, P. (1990) Two distinct estrogen-regulated promoters generate transcripts encoding the two functionally different human progesterone receptor forms A and B, *EMBO J. 9*, 1603−14.
3. Meyer, M. E., Quirin-Stricker, C., Lerouge, T., Bocquel, M. T., and Gronemeyer, H. (1992) A limiting factor mediates the differential activation of promoters by the human progesterone receptor isoforms, *J. Biol. Chem. 267*, 10882−7.
4. Sartorius, C. A., Melville, M. Y., Hovland, A. R., Tung, L., Takimoto, G. S., and Horwitz, K. B. (1994) A third transactivation function (AF3) of human progesterone receptors located in the unique N-terminal segment of the B-isoform, *Mol. Endocrinol. 8*, 1347−60.
5. Meyer, M. E., Pornon, A., Ji, J. W., Bocquel, M. T., Chambon, P., and Gronemeyer, H. (1990) Agonistic and antagonistic activities of RU486 on the functions of the human progesterone receptor, *EMBO J. 9*, 3923−32.
6. Mulac-Jericevic, B., Mullinax, R. A., DeMayo, F. J., Lydon, J. P., and Conneely, O. M. (2000) Subgroup of reproductive functions of progesterone mediated by progesterone receptor-B isoform, *Science 289*, 1751−4.
7. Mulac-Jericevic, B., Lydon, J. P., DeMayo, F. J., and Conneely, O. M. (2003) Defective mammary gland morphogenesis in mice lacking the progesterone receptor B isoform, *Proc. Natl. Acad. Sci. U.S.A. 100*, 9744−9.
8. Richer, J. K., Jacobsen, B. M., Manning, N. G., Abel, M. G., Wolf, D. M., and Horwitz, K. B. (2002) Differential gene regulation by the two progesterone receptor isoforms in human breast cancer cells, *J. Biol. Chem. 277*, 5209−18.
9. Hopp, T. A., Weiss, H. L., Hilsenbeck, S. G., Cui, Y., Alfred, D. C., Horwitz, K. B., and Fuqua, S. (2004) Breast cancer patients with progesterone receptor PR-A-rich tumors have poorer disease-free survival rates, *Clin. Cancer Res. 15*, 2751−60.
10. DeMarzo, A. M., Beck, C. A., Onate, S. A., and Edwards, D. P. (1991) Dimerization of Mammalian Progesterone Receptors Occurs in the Absence of DNA and is Related to the Release of the 90-kDa Heat Shock Protein, *Proc. Natl. Acad. Sci. U.S.A. 88*, 72−6.
11. Rodriguez, R., Weigel, N. L., O'Malley, B., and Schrader, W. T. (1990) Dimerization of the chicken progesterone receptor in vitro can occur in the absence of hormone and DNA, *Mol. Endocrinol. 4*, 1782−90.
12. Beckett, D. (2001) Regulated assembly of transcription factors and control of transcription initiation, *J. Mol. Biol. 314*, 335−52.
13. Senear, D. F., Ross, J. B., and Laue, T. M. (1998) Analysis of protein and DNA-mediated contributions to cooperative assembly of protein-DNA complexes, *Methods 16*, 3−20.

14. Heneghan, A. F., Berton, N., Miura, M. T., and Bain, D. L. (2005) Self-Association Energetics of an Intact, Full-Length Nuclear Receptor: The B-Isoform of Human Progesterone Receptor Dimerizes in the Micromolar Range, *Biochemistry 44*, 9528−37.
15. Heneghan, A. F., Connaghan-Jones, K. D., Miura, M. T., and Bain, D. L. (2006) Cooperative DNA Binding by the B-Isoform of Human Progesterone Recptor: Thermodynamic Analysis Reveals Strongly Favorable and Unfavorable Contributions to Assembly, *Biochemistry 45*, 3285−96.
16. Perlmann, T., Eriksson, P., and Wrange, O. (1990) Quantitative Analysis of the Glucocorticoid Receptor-DNA Interaction at the Mouse Mammary Tumor Virus Glucocorticoid Response Element, *J. Biol. Chem. 265*, 17222−9.
17. Segard-Maurel, I., Rajkowski, K., Jibard, N., Schweizer-Groyer, G., Baulieu, E.-E., and Cadepond, F. (1996) Glucocorticoid Receptor Dimerization Investigated by Analysis of Receptor Binding to Glucocorticosteroid Responsive Elements Using a Monomer-Dimer Equilibrium Model, *Biochemistry 35*, 1634−42.
18. Tanmrazi, A., Carlson, K. E., Daniels, J. R., Hurth, K. M., and Katzenellenbogen, J. A. (2002) Estrogen receptor dimerization: Ligand binding regulates dimer affinity and dimer dissociation rate, *Mol. Endocrinol. 16*, 2706.
19. Christensen, K., Estes, P. A., Onate, S. A., Beck, C. A., DeMarzo, A., Altmann, M., Lieberman, B. A., St John, J., Nordeen, S. K., and Edwards, D. P. (1991) Characterization and functional properties of the A and B forms of human progesterone receptors synthesized in a baculovirus system, *Mol. Endocrinol. 5*, 1755−70.
20. Tetel, M. J., Giangrande, P. H., Leonhardt, S. A., McDonnell, D. P., and Edwards, D. P. (1999) Hormone-dependent interaction between the amino- and carboxyl-terminal domains of progesterone receptor in vitro and in vivo, *Mol. Endocrinol. 13*, 910−24.
21. Gill, S., and von Hippel, P. (1989) Calculation of protein extinction coefficients from amino acid sequence data, *Anal. Biochem. 182*, 319−26.
22. Philo, J. S. (2000) A Method for Directly Fitting the Time Derivative of Sedimentation Velocity Data and an Alternative Algorithm for Calculating Sedimentation Coefficient Distribution Functions, *Anal. Biochem. 279*, 151−63.
23. Stafford, W. F. (1992) Boundary analysis in sedimentation transport experiments: A procedure for obtaining sedimentation coefficient distributions using the time derivative of the concentration profile, *Anal. Biochem. 203*, 295−301.
24. Van Holde, K. E. (1971) *Physical Biochemistry*, Prentice Hall, Englewood Cliffs, CA.
25. Schuck, P. (2003) On the Analysis of Protein Self-Association by Sedimentation Velocity Analytical Ultracentrifugation, *Anal. Biochem. 320*, 104−24.
26. Cohn, E. J., and Edsall, J. T. (1943) *Proteins, Amino Acids and Peptides*, Reinhold, New York.
27. Passen, H., and Kumosinski, T. F. (1985) Measurements of protein hydration by various techniques, *Methods Enzymol. 117*, 219−55.
28. Waxman, E., Laws, W. R., Laue, T. M., Nemerson, Y., and Ross, J. B. A. (1993) Human factor VIIa and its complex with soluble tissue factor: Evaluation of symmetry and conformational dynamics by ultracentrifugation and fluoresence anisotropy decay methods, *Biochemistry 32*, 3005−12.
29. Johnson, M. L., Correia, J. J., Yphantis, D. A., and Halvorson, H. R. (1981) Analysis of data from the analytical ultracentrifuge by nonlinear least-squares techniques, *Biophys. J. 36*, 575−88.
30. Laue, T. M., Shah, B. D., Ridgeway, T. M., and Pelletier, S. L. (1992) *Analytical Ultracentrifugation in Biochemistry and Polymer Science*, Royal Society of Chemistry, Cambridge, U.K.
31. Smith, D. F., Lubahn, D. B., McCormick, D. J., Wilson, E. M., and Toft, D. O. (1988) The production of antibodies against the conserved cysteine region of steroid receptors and their use in characterizing the avian progesterone receptor, *Endocrinology 122*, 2816−25.
32. Bain, D. L., Franden, M. A., McManaman, J. L., Takimoto, G. S., and Horwitz, K. B. (2000) The N-terminal region of the human progesterone A-receptor: Structural analysis and the influence of the DNA binding domain, *J. Biol. Chem. 275*, 7313−20.
33. Bain, D. L., Franden, M. A., McManaman, J. L., Takimoto, G. S., and Horwitz, K. B. (2001) The N-terminal region of human progesterone B-receptors: Biophysical and biochemical comparison to A-receptors, *J. Biol. Chem. 276*, 23825−31.
34. Williams, S. P., and Sigler, P. B. (1998) Atomic structure of progesterone complexed with its receptor, *Nature 393*, 392−6.
35. Theofan, G., and Notides, A. C. (1984) Characterization of the calf uterine progesterone receptor and its stabilization by nucleic acids, *Endocrinology 114*, 1173−9.
36. Brodie, J., and McEwan, I. J. (2005) Intra-domain communication between N-terminal and DNA-binding domains of the androgen receptor: Modulation of androgen response element DNA binding, *J. Mol. Endocrinol. 34*, 603−15.
37. Kumar, R., and Thompson, E. B. (2003) Transactivation Functions of the N-terminal Domains of Nuclear Hormone Receptors: Protein Folding and Coactivator Interactions, *Mol. Endocrinol. 17*, 1−10.
38. Warnmark, A., Treuter, E., Wright, A. P. H., and Gustafsson, J.-A. (2003) Activation Functions 1 and 2 of Nuclear Receptors: Molecular Strategies for Tanscriptional Activation, *Mol. Endocrinol. 17*, 1901−9.
39. Takimoto, G. S., Tung, L., Abdel-Hafiz, H., Abel, M. G., Sartorius, C. A., Richer, J. K., Jacobsen, B. M., Bain, D. L., and Horwitz, K. B. (2003) Functional properties of the N-terminal region of progesterone receptors and their mechanistic relationship to structure, *J. Steroid Biochem. Mol. Biol. 85*, 209−19.
40. Mohamed, M. K., Tung, L., Takimoto, G. S., and Horwitz, K. B. (1994) The leucine zippers of c-fos and c-jun for progesterone receptor dimerization: A-dominance in the A/B heterodimer, *J. Steroid Biochem. Mol. Biol. 51*, 241−50.

BI0612317